Understanding magnetic interactions in the series $A_2FeX_5 \cdot H_2O$ (A=K, Rb; X=Cl, Br). I. Spin densities by polarized neutron diffraction and DFT calculations

Javier Luzón,[1,*] Javier Campo,[1,†] Fernando Palacio,[1] Garry J. McIntyre,[2] and Angel Millán[1]
[1]*Instituto de Ciencia de Materiales de Aragón, CSIC and Universidad de Zaragoza, Pedro Cerbuna 12, 50009 Zaragoza, Spain*
[2]*Institut Laue-Langevin, 6 Rue Jules Horowitz, 38042 Grenoble, France*
(Received 19 February 2008; revised manuscript received 10 July 2008; published 11 August 2008)

The compounds $A_2FeX_5 \cdot H_2O$ (A=alkali or NH_4; X=Cl, Br) form a series of collinear antiferromagnets with transition temperatures in the range from 6 to 23 K. These ordering temperatures are much higher than in other hydrated salts of transition-metal ions with similar distances between magnetic ions. Spin-density distributions have been determined in $Rb_2FeBr_5 \cdot H_2O$ and $K_2FeCl_5 \cdot H_2O$ by means of the polarized-neutron-diffraction technique and *ab initio* calculations in order to elucidate the mechanism of such enhancement. The results show a large spin-density delocalization (~20%) toward the ligand atoms, which explains the efficiency of the superexchange pathways in transmitting the magnetic interaction.

DOI: 10.1103/PhysRevB.78.054414 PACS number(s): 75.50.Xx, 75.30.Et, 71.15.Mb

I. INTRODUCTION

The series of compounds $A_2FeX_5 \cdot H_2O$ (A=alkali or NH_4; X=Cl, Br) was extensively studied in the past due to the high interest in several magnetic phenomena present in the series: They are all isostructural and consist of $[FeX_5 \cdot H_2O]^{-2}$ octahedra linked together in the structural packing by a network of hydrogen bonds.[1] The low magnetic anisotropy of these collinear antiferromagnets makes them quasi-ideal model examples of the Heisenberg Hamiltonian, which permitted the verification of theoretical predictions for lattice dimensionality crossover.[2,3] Moreover, the phase diagrams of these compounds include a well-defined spin-flop transition.[4,5] When a small fraction of the Fe ions are substituted by diamagnetic In, a large broadening of the antiferromagnetic to spin-flop phase boundary is observed and an intermediate phase predicted by Fishman and Aharony[6] has been suggested.[7,8] Another very striking magnetic phenomenon observed in this series is the remanent magnetization that appears below the antiferromagnetic transition temperature T_N. This remanent magnetization, which has also been observed in other low-anisotropy diluted antiferromagnets,[9–13] can be scaled to a universal curve independent of the compound.

Despite the interest in and the so far achieved understanding of the magnetism of these compounds, there remains a basic question that has not yet been answered: In these compounds the superexchange pathways are very long, on the order of 7–8 Å, and include two diamagnetic intermediaries (or three if a H bond is included) of the types Fe–$X\cdots X$–Fe and Fe–O$\cdots X$–Fe. However, they are surprisingly effective in transmitting the magnetic interactions, which results in relatively high transition temperatures (see Table I) that are about 1 order of magnitude higher than those of other hydrated halides, such as $Cs_2FeCl_5 \cdot 4H_2O$ [T_c=0.185 K (Ref. 18)], $Cs_2MnCl_4 \cdot 2H_2O$ [T_c=1.8 K (Ref. 19)], and $K_2FeF_5 \cdot H_2O$ [T_c=0.8 K (Ref. 20)], for the same type of superexchange pathways.

A likely hypothesis for such anomalously intense superexchange magnetic interactions is a delocalization of some spin density from the iron ions to the ligands due to covalent bonding. In fact, electron-transfer transitions from chloride-centered nonbonding and antibonding orbitals to metal-centered t_{2g} and e_g orbitals have been observed in the wavelength range 500–300 nm in $(NH_4)_2Fe_xIn_{1-x}Cl_5H_2O$.[21] Recent ^{35}Cl NMR studies in single crystals of $K_2FeCl_5H_2O$ observed four different internal fields in the Cl atoms,[22] the largest one being assigned to the chlorine atom involved in the strongest superexchange pathway according to previous magnetostructural correlation analysis.[3]

The knowledge of the spin-density distribution is of crucial importance in the understanding of the magnetic interaction mechanisms. This is particularly so in molecular magnetic systems where spin moments can be delocalized at the molecular level.[23–25] In particular, in the $A_2FeX_5 \cdot H_2O$ series this knowledge would allow determination of whether the relatively high magnetic transition temperatures are due to an important spin delocalization from the iron ion toward the ligand atoms, as proposed in the previous paragraph. The existence of such a spin delocalization, which would strengthen the interaction between magnetic orbitals localized in different octahedra, is also supported by a reduced magnetic moment observed at the iron site in a powder-neutron-diffraction experiment on $K_2FeCl_5 \cdot H_2O$.[26]

In this paper we report the analysis of the spin-density distribution in $K_2FeCl_5 \cdot H_2O$ and $Rb_2FeBr_5 \cdot H_2O$ using two complementary methods: polarized neutron diffraction (PND) and density-functional-theory (DFT) calculations. This analysis will contribute to elucidation of two important

TABLE I. Néel temperatures T_N for the $A_2FeX_5 \cdot H_2O$ series.

A,X	NH_4,Cl	Cs,Cl	Rb,Cl	K,Cl	Cs,Br	Rb,Br
T_N	7.25	6.54	10.00	14.06	14.20	22.90
Reference	14	15 and 16	15 and 16	14	17	17

open questions necessary to understand the mechanism of the magnetic interactions in these compounds: the extent to which the spin is delocalized from the iron atom toward the halogen atoms and the oxygen atom and, related to the first point, the reason why magnetic interactions are stronger in the bromide derivatives than in the chloride derivatives. Moreover, the knowledge of the spin density will allow us in a second paper[27] to understand the role played by the hydrogen bond in the magnetic interactions.

The spin-density delocalization from the metal ion toward the ligand atoms has already been studied in a large number of 3*d* transition-metal complexes by PND in order to obtain information about the metal-ligand bonding nature. An early review can be found in Ref. 28. In particular, the ammonium Tutton salt series $(NH_4)_2M(SO_4)_2\cdot 6H_2O$ (M=transition metal) has been extensively studied in order to understand the covalence between the transition-metal and the ligand atoms as a function of the transition metal.[29–34] In the Tutton salts of 3*d* transition metals, including the iron Tutton salt, there is only a slight spin delocalization from the transition metal toward the water molecules. Slight spin delocalization effects, below $0.07\mu_B$ per ligand atom, have also been observed in several well-isolated 3*d* transition-metal halide complexes studied by PND.[35–37] As for iron compounds, in a Fe^{2+} compound, FeF_2, there is a 10% spin delocalization from the iron ion[38] and in a $[FeCl_4]^-$ complex the spin population of the chlorine atoms is around $0.15\mu_B$.[39] This last result supports the hypothesis of an important spin delocalization to the ligand atoms in the $A_2FeX_5\cdot H_2O$ series, although one should remember that the Fe^{3+} is in a different environment.

After this introductory section, Sec. II will be devoted to the experimental determination of the spin-density distributions in $K_2FeCl_5\cdot H_2O$ and $Rb_2FeBr_5\cdot H_2O$. This part includes the description of the neutron-diffraction experiments as well as a detailed analysis of the data using different approaches (maximum-entropy method[40] and the multipole expansion approach[41]). In Sec. III, the results of the *ab initio* calculations are presented. Finally, conclusions will be stated in Sec. IV.

II. EXPERIMENTAL DETERMINATION OF THE SPIN-DENSITY DISTRIBUTION

The magnetic structure factors are related to the Fourier transform of the magnetization density. Therefore, the precise measurement of the magnetic structure factors, including the phases, can be used for the determination of the magnetization density distribution.

The combination of polarized neutrons and the flipping ratio measurement method increases the sensibility of the neutron-diffraction experiments for the measurement of the magnetic structure factors. In this technique, the measured quantity for a Bragg peak is the ratio of the intensities diffracted for an incident-neutron beam with polarization along the up or the down vertical direction, with the sample in a single-domain ferromagnetic magnetized state, induced typically by a vertical magnetic field:

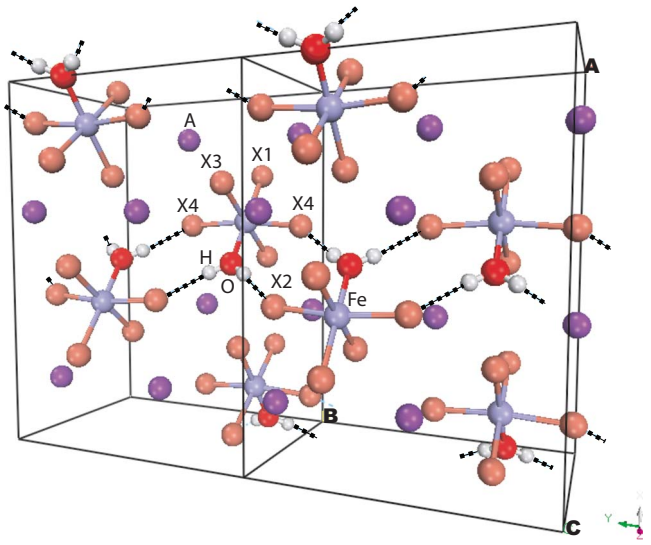

FIG. 1. (Color online) Schematic of the crystallographic structure of the $A_2FeX_5\cdot H_2O$ compounds with *Pnma* as space group.

$$R = \frac{I^+}{I^-} = \frac{|F_N + F_M|^2}{|F_N - F_M|^2}, \tag{1}$$

where F_N and F_M are, respectively, the nuclear and the magnetic structure factors. In the case of a centrosymmetric structure, the magnetic structure factor, including its phase, can be extracted from Eq. (1) if the nuclear structure factor is known.

A. Nuclear structure determination

$Cs_2FeCl_5\cdot H_2O$ crystallizes in the *Cmcm* space group.[15] All the other compounds of the series are isomorphous and belong to the *Pnma* space group.[1] A schema of the structure of the compounds in the *Pnma* space group is represented in Fig. 1, where the labeling used throughout this paper for the halogen atoms is shown. The unit cell contains four discrete $[FeX_5\cdot H_2O]^{2-}$ octahedra connected by hydrogen bonds. In each octahedron three halogen atoms, the oxygen atom, and the iron atom are in special positions 4*c* with point symmetry *m* and the other atoms are in general positions. The octahedra are arranged in planes perpendicular to the *b* axis and the hydrogen bonds connect octahedra related by the inversion operator to form chains along the *b* axis.

In the case of the studied compounds, the nuclear structure of $K_2FeCl_5\cdot H_2O$ was already known from a single-crystal x-ray-[42] and powder-neutron-diffraction experiments,[26,43] while the nuclear structure of $Rb_2FeBr_5\cdot H_2O$ was known only from x-ray experiments at room temperature.[17] Since the hydrogen atoms are supposed to play an important role in the magnetic interactions of these compounds, their location is of particular interest. In an x-ray-diffraction experiment the hydrogen atoms are difficult to locate precisely when other much heavier atoms such as iron, potassium, rubidium, or bromine are in the lattice. This is not the case in neutron-diffraction experiments. Moreover, the analysis of the flipping ratios in the polarized-neutron-diffraction experiment requires an accurate knowledge of the

TABLE II. Data collection conditions and unit-cell parameters in the low-temperature nuclear structure determinations of $K_2FeCl_5 \cdot H_2O$ and $Rb_2FeBr_5 \cdot H_2O$.

Compound	$K_2FeCl_5 \cdot H_2O$	$Rb_2FeBr_5 \cdot H_2O$
Crystal size (mm^3)	$1 \times 3 \times 5$	$1 \times 3 \times 4$
Diffractometer	D9 (ILL)	D10 (ILL)
Monochromator	Cu(2 2 0)	Cu(2 0 0)
Wavelength (Å)	0.8426(1)	1.2594(4)
Cryogenic environment	Cryorefrigerator	He-flow cryostat
Temperature (K)	20	30
Scan mode	ω	ω
sin θ/λ maximum ($Å^{-1}$)	0.50	0.74
Measured reflections	1768	2357
Unique reflections	447	1857
Cell parameters (Å)		
a	13.4838(6)	14.2540(4)
b	9.6454(4)	10.2898(3)
c	7.0011(3)	7.3746(2)

TABLE III. Refinement conditions and agreement factors in the low-temperature structure determinations of $K_2FeCl_5 \cdot H_2O$ and $Rb_2FeBr_5 \cdot H_2O$.

Compound	(K,Cl)	(Rb,Br)
Number of variables	59	59
Absorption coefficient (cm^{-1})	0.6261	0.1656
Extinction parameters		
Domain radius (fixed) (μm)	100	100
Mosaic spread (10^{-4} rad^{-1})	0.1858(48)	0.1713(31)
Agreement factors		
R	0.018	0.035
R_w	0.012	0.023
χ^2	8.99	2.14

nuclear structure and the characteristics of the particular sample studied. Consequently two single-crystal nonpolarized-neutron-diffraction experiments were performed on $K_2FeCl_5 \cdot H_2O$ and $Rb_2FeBr_5 \cdot H_2O$.

The experimental conditions for each compound are reported in Table II. The experiment on $K_2FeCl_5 \cdot H_2O$ was carried out on the four-circle diffractometer D9 at the Institut Laue-Langevin (ILL). The $1 \times 3 \times 5$ mm^3 single crystal intended for the later PND experiment was cooled in a cryorefrigerator down to 20 K, a temperature that is above the magnetic transition temperature of 14.06 K. This temperature was chosen to be not too close to the transition temperature in order to avoid the short-range antiferromagnetic correlations. The Cu(2 2 0) plane used to monochromize the neutron beam provided a wavelength of 0.8426(1) Å. The $Rb_2FeBr_5 \cdot H_2O$ single crystal of $1 \times 3 \times 4$ mm^3 dimensions was measured on the four-circle diffractometer D10 at the ILL at 30 K, also above the magnetic transition temperature of 22.90 K. In this case a wavelength of 1.2594(4) Å was provided by a Cu(2 0 0) crystal.

The integration of the peak intensities was performed using the ILL RACER program. In the D9 experiment 1768 reflections extending to sin $\theta/\lambda = 0.50$ $Å^{-1}$ were merged into 447 unique reflections, while in the D10 experiment a total of 2357 reflections extending to sin $\theta/\lambda = 0.74$ $Å^{-1}$ were merged into 1857 unique reflections.

Programs from the CCSL suite[44] were used to process the data. The absorption correction for the hydrogen atom requires special attention. In general, the incoherent neutron-scattering cross section is supposed to be constant. However, in the case of the hydrogen atom a dependence on the wavelength has been observed in neutron-diffraction experiments.[45] The incoherent-neutron-scattering cross section for the hydrogen atoms in both experiments were estimated from the fit of such dependence in compounds with similar hydrogen environments. The obtained absorption coefficients were 0.6261 and 0.1656 cm^{-1} for the chloride and bromide compounds, respectively, at the wavelengths used.

The least-squares refinement program SFLSQ from the CCSL suite was used to refine the scale factor, the atom positions, the anisotropic thermal parameters, and the mosaic spread for the isotropic secondary extinction correction.[46] These parameters were optimized against the square of the structure amplitudes ($|F_N^2|$) using $1/\sigma^2$ as statistical weight to fit the reflections, where σ is the standard deviation of the reflection intensity. The refinement conditions and agreement factors[47] are listed in Table III. The fractional atomic positions and the anisotropic thermal parameters[48] obtained for both compounds are reported in Tables IV and V.

One of the factors that are supposed to play an important role in the amount of the spin-density delocalization from the iron ion toward the ligand atoms is the ligand bond length. Bond lengths for the coordination sphere of the iron ion in both compounds are listed in Table VI.

The Fe-O bond is the shortest iron-to-ligand distance in each compound, whereas the shortest Fe-*X* bond is between the iron and the halogen atoms in *trans* positions with respect to the oxygen atom. The bond lengths between the iron atom and the four halogen atoms in the plane perpendicular to the O-Fe-*X* axis of the coordination octahedron are all very similar in each compound.

B. PND experiments

Polarized-neutron-diffraction experiments were performed on instrument D23 at the ILL on the same crystals and at the same temperatures as in the nonpolarized-neutron-diffraction experiments. Both compounds have been measured above their antiferromagnetic order temperatures, in order to avoid the antiferromagnetic ordering of the spins. Therefore the highest magnetic field, 5.5 T, provided by the cryomagnet was employed in order to maximize the magnetization in the paramagnetic phase. A pyrolytic graphite (0 0 2) crystal and a Heusler (1 1 1) polarizer were used to monochromate and polarize the incoming neutron beam. The monochromatic beams were at nominal wavelengths of 1.3293(1) and 1.2779(1) Å, respectively, for the chlorine and the bromine experiments, with a polarization of 0.95 in both experiments. A flipper with 98% efficiency reversed the

TABLE IV. Fractional positions and anisotropic thermal parameters for $K_2FeCl_5 \cdot H_2O$ at 20 K.

Atom	x	y	z	β_{11}	β_{22}	β_{33}	β_{23}	β_{13}	β_{12}
K	0.354 23(13)	0.498 12(19)	0.146 14(25)	0.575(77)	0.627(79)	0.416(92)	0.063(67)	0.090(74)	0.027(58)
Fe	0.114 39(07)	0.25	0.194 04(15)	0.174(50)	0.202(40)	0.234(49)	0	−0.045(42)	0
Cl1	0.252 37(12)	0.25	0.395 71(14)	0.275(51)	0.455(46)	0.261(50)	0	−0.078(43)	0
Cl2	0.218 78(07)	0.25	−0.078 33(15)	0.387(51)	0.547(46)	0.245(51)	0	0.069(41)	0
Cl3	0.006 14(07)	0.25	0.467 45(14)	0.396(51)	0.448(43)	0.349(49)	0	0.090(40)	0
Cl4	0.104 42(05)	0.496 35(14)	0.185 96(10)	0.454(37)	0.265(28)	0.426(34)	0.015(28)	−0.111(29)	0.028(21)
O	−0.008 98(15)	0.25	0.016 14(31)	0.17(10)	0.70(12)	0.69(11)	0	−0.224(85)	0
H	−0.035 98(17)	0.331 62(30)	−0.044 61(35)	2.04(11)	1.63(14)	2.19(12)	0.50(11)	−0.591(95)	0.231(95)

polarization between parallel and antiparallel with respect to the direction of the vertical magnetic field applied to the samples.

In each experiment the single crystal was mounted in two different orientations to gain access to the maximum number of Bragg reflections in order to overcome the limited access in one setting in normal-beam geometry. For $K_2FeCl_5 \cdot H_2O$ a total of 161 and 180 flipping ratios were measured with, respectively, the crystal axes [0 0 1] and [0 1 0] parallel to the applied vertical magnetic field. Similarly, 137 and 189 reflections were measured for $Rb_2FeBr_5 \cdot H_2O$ with the [1 0 0] and [0 0 1] axes vertically, respectively.

Programs of the CCSL suite were employed to extract the magnetic structure factors from the measured flipping ratios using the nuclear structures and parameters from the nonpolarized-neutron-diffraction experiments. In these compounds the Fe^{3+} ground term is $^6A_1$ with the five $3d$ electrons in a high-spin configuration $t_{2g}^3 e_g^2$ ($S=5/2$). Since this ground state is an orbital singlet, there is no need to account for the orbital contribution to the magnetization distribution, which otherwise would have been dependent on the direction of the applied magnetic field. Moreover, the magnetic anisotropy is quite low in these compounds,[1] so it was possible to merge the magnetic structure factors measured in the two directions, resulting in 271 and 282 unique reflections for the chloride and bromide compounds, respectively. The analysis of the spin-density distribution from the magnetic structure factors obtained in the polarized-neutron-diffraction experiment were performed using two different approaches: the maximum-entropy method and an analytical fit of the magnetic structure factors, in which the spin-density distribution is modeled by a multipole expansion around the atoms.

C. Maximum-entropy method

The maximum-entropy method[40] allows the reconstruction of the spin-density distribution without applying any model and, unlike the straightforward inverse Fourier transform, is suitable for the treatment of noisy and significantly incomplete data. Brillouin's law for a 5/2 spin at the conditions of magnetic field and temperature of the PND experiments gives $1.99\mu_B$ and $1.38\mu_B$ for the magnetic moments of the iron ion in the chloride and the bromide compounds. These values are far below the $5\mu_B$ of the saturation, which implies low magnetic signals and consequently noisy data. Therefore, we started the study of the spin-density distribution with the maximum-entropy method to have an idea of the spin density before introducing any model.

The maximum-entropy reconstructions of the spin densities were performed using the CCSL program MAGMAX3D, which is based on the MEMSYS3 package.[49] The (asymmetric) $0.5a \times 0.5b \times 1.0c$ unit-cell fraction was digitized on a $32 \times 24 \times 32$ grid to achieve an approximate resolution of 0.2 Å per pixel along each crystallographic axis.

The resulting spin densities were normalized to $20\mu_B$ per unit cell in order to facilitate the comparison. Figures 2(a) and 2(b) show the maximum-entropy-reconstructed spin densities projected onto a plane containing atoms Fe, O, and $X4$. This plane also contains the hydrogen bond, which is supposed to play an important role in the transmission of the magnetic interaction. The projection was made with a thickness of 4 Å, in each side of the projection plane to account for all the spin density of the octahedron.

TABLE V. Fractional positions and anisotropic thermal parameters for $Rb_2FeBr_5 \cdot H_2O$ at 30 K.

Atom	x	y	z	β_{11}	β_{22}	β_{33}	β_{23}	β_{13}	β_{12}
Rb	0.356 44(03)	0.498 31(05)	0.156 60(06)	0.316(14)	0.349(14)	0.415(16)	0.009(13)	0.040(11)	−0.005(12)
Fe	0.114 77(03)	0.25	0.196 59(07)	0.235(14)	0.204(15)	0.265(17)	0	−0.028(13)	0
Br1	0.251 38(05)	0.25	0.404 39(09)	0.182(19)	0.274(21)	0.266(22)	0	−0.011(18)	0
Br2	0.222 40(05)	0.25	−0.073 15(10)	0.350(21)	0.298(22)	0.274(23)	0	0.023(18)	0
Br3	0.005 02(05)	0.25	0.469 48(10)	0.205(20)	0.296(21)	0.362(25)	0	0.057(19)	0
Br4	0.102 88(03)	0.496 24(05)	0.181 63(07)	0.270(14)	0.223(14)	0.375(16)	0.017(13)	−0.052(12)	0.000(12)
O	−0.002 95(06)	0.25	0.023 62(13)	0.476(25)	0.425(28)	0.816(33)	0	−0.304(24)	0
H	−0.027 63(10)	0.326 25(13)	−0.033 76(22)	2.521(51)	1.283(43)	2.688(59)	0.580(43)	−0.928(45)	0.376(40)

TABLE VI. Bond lengths (Å) for $K_2FeCl_5 \cdot H_2O$ at 20 K and for $Rb_2FeBr_5 \cdot H_2O$ at 30 K.

	$K_2FeCl_5 \cdot H_2O$	$Rb_2FeBr_5 \cdot H_2O$
Fe-*X*1	2.3355(24)	2.4779(12)
Fe-*X*2	2.3701(20)	2.5121(12)
Fe-*X*3	2.4071(20)	2.5490(63)
Fe-*X*4	2.3806(13)	2.5418(05)
Fe-O	2.0781(31)	2.1078(14)
O-H	0.9660(35)	0.9583(18)

The spin-density projection for $K_2FeCl_5 \cdot H_2O$ confirms that there is an important spin-density delocalization from the iron atom to the ligand atoms. The highest spin delocalization is to the chlorine atom opposite to the oxygen atom, which is an expected result because it is the chlorine atom with the shortest Fe-Cl bond. On the other hand, the spin-density delocalization toward all the chlorine atoms seems to be higher than toward the oxygen atom.

The spin delocalization is supposed to be higher in the bromine compound than in the chlorine one because the electronegativity difference between the iron ion and the halide anion is lower, which favors covalency. However, surprisingly, the reconstructed spin-density projection for $Rb_2FeBr_5 \cdot H_2O$ shows virtually no spin delocalization. The reason is that the experimental magnetic structure factors for the bromide compound are noisier because the experiment was performed at 30 K. This noise does not allow the ligand spin densities to be differentiated from the much higher iron spin density. Instead, an elongation of the iron spin density toward the ligand atoms is observed, especially toward the Br1 atom, an atom which is supposed to show the highest spin delocalization. The only ligand atom around which a distinct spin density is observed is the Br4 atom. This atom is the only ligand which is not in a 4*c* special position but in a general position. The magnetic structure factors that are systematically extinct for the 4*c* special position are due almost solely to the spin density of the Br4 atom. In the maximum-entropy language, the experimental data contain more information about the spin density of the Br4 atoms than about the spin density of the other ligand atoms, allowing this spin density to be distinguished from the iron spin density. Another reason favoring the detection by maximum entropy of the Br4 spin density is related to symmetry: There are two Br4 atoms per octahedron, so its contribution to the magnetic signal is double than that of the other bromides.

This *softening* of the spin-density distribution is a typical behavior of the maximum-entropy method, which chooses the solution with less information, thus tending to hide weak features near stronger features. That is also the reason why the spin density of the chlorine atoms in $K_2FeCl_5 \cdot H_2O$ is not exactly at the chlorine atom position but between the chlorine and the iron atom positions.

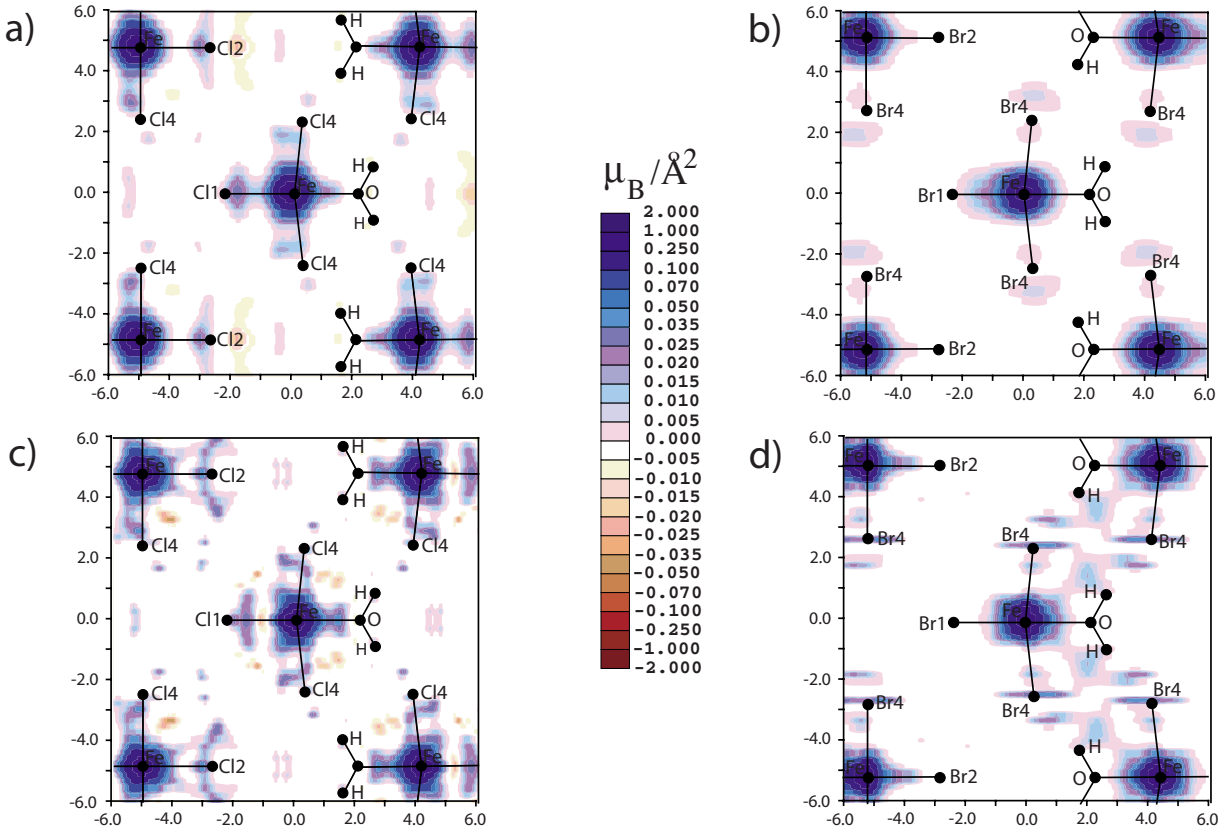

FIG. 2. (Color online) Projection of the maximum-entropy-reconstructed spin-density distribution for $K_2FeCl_5 \cdot H_2O$ and $Rb_2FeBr_5 \cdot H_2O$.The projection plane contains the Fe, O, and *X*4 atoms. (a) $K_2FeCl_5 \cdot H_2O$ with a uniform prior; (b) $Rb_2FeBr_5 \cdot H_2O$ with a uniform prior; (c) $K_2FeCl_5 \cdot H_2O$ with a nonuniform prior; (d) $Rb_2FeBr_5 \cdot H_2O$ with a nonuniform prior.

In the above maximum-entropy analysis, the default model of the spin density was a uniform distribution throughout the asymmetric unit. In other words, no prior knowledge of the spin density was supposed. The use of an adequate nonuniform default model allows discernment between the real and spurious features of a spin-density distribution. This nonuniform prior density must not contain such features, so only real features are likely to survive against this negative bias. The chosen prior spin densities are spherical spin-density distributions around the iron atom with a magnetic moment per iron ion as predicted by the Brillouin function for a 5/2 spin at the temperatures and the magnetic fields of the experiments. The radial part of these spherical distributions is a Slater functional $r^n \exp(-\alpha r)$ with $n=6$ and $\alpha=7.44$. These are spin-density distributions biased against the delocalization of spin density toward the halogen atoms in order to check whether the spin delocalizations observed using the uniform default model are real or only spurious effects.

Figures 2(b) and 2(c) present the maximum-entropy-reconstructed spin densities using the nonuniform priors projected onto the same two planes as in the case of the uniform prior. The projection was again made with a thickness of 4 Å, on each side of the projection plane.

In the case of $K_2FeCl_5 \cdot H_2O$, the reconstructed spin density using a nonuniform prior is very similar to the spin density with a uniform prior, although the spin density of the ligand atoms is better resolved from the spin density of the iron atom, especially for the oxygen atom. Therefore, this analysis confirms the existence of a spin delocalization from the iron ion toward the ligand atoms.

In $Rb_2FeBr_5 \cdot H_2O$, the ligand spin densities continue to be almost absorbed in the spin density of the iron atom. Nevertheless, the elongations of the spin density toward the halogen atoms are bigger except for the Br4 site, for which the spin-density elongation has disappeared. These elongations also indicate a spin delocalization which is hidden in the maximum-entropy method due to the noise of the data.

To sum up, the maximum-entropy method indicates that there can be an important spin delocalization from the iron atom toward the ligand atoms. This spin delocalization is higher toward the halogen atoms than toward the oxygen atom. In Sec. II D, the use of a model will allow us to quantify this spin-density delocalization.

D. Multipole expansion approach

Two different approaches are commonly used to fit analytically the magnetic structure factors by modeling the spin-density distribution. In the first one, called the multipole expansion approach,[41] the spin-density distribution is modeled by a multipole expansion centered on the atoms. In the second one, called the wave-function approach,[50] the spin-density distribution is obtained as the square of a wave function composed of atomic orbitals. It is worthwhile to note that the multipole expansion approach can be transformed to the wave-function approach by introducing constraints among the multipole coefficients.

For the Fe^{3+} ion, the wave-function approach would allow us to account for the different populations of the $3d$ orbitals but not for the spin-density distortion due to the ligand crystal field, where a water molecule instead of a halogen atom is on one vertex of the octahedron. Since all the $3d$ orbitals are semioccupied, the main spin population difference would be between e_g and t_{2g} orbitals. This effect on the spin-density distribution will be lower than the spin-density deformation produced by the ligand crystal field. Therefore, the wave-function approach is not suitable for modeling the spin-density distribution and the multipole expansion approach was chosen.

TABLE VII. ζ and n exponents for the radial component in the multipolar expansion.

Atom	ζ	n
Fe	7.44	6
Cl	4.08	4
Br	4.51	6
O	4.55	2

As stated above, in the multipole expansion approach the spin density is partitioned into separate atomic contributions which are expanded on the basis of the real spherical harmonics d_{lm}, which are also referred to as multipoles

$$m(\vec{r}) = \sum_{i}^{\text{atoms}} \sum_{l} R_i^{l,\text{dens}}(|\vec{r}-\vec{r}_i|) \sum_{m=-l}^{m=l} P_{ilm} d_{lm}(\theta_i, \varphi_i). \quad (2)$$

P_{ilm} are the population coefficients of the real spherical harmonics $d_{lm}(\theta_i, \varphi_i)$ and $R_i^{l,\text{dens}}(r)$ are radial functions which usually are Slater functions:

$$R_i^{l,\text{dens}}(r) = \frac{\zeta^{n_{il}+3}}{(n_{il}+2)!} r^{n_{il}} \exp(-\zeta_{il} r), \quad (3)$$

where the coefficients n_{il} may be selected by examination of the orbitals that originate the spin-density distribution. E.g., in a spin-density distribution from a $3p$ orbital, n_{il} will be $(3-1)\times 2 \rightarrow 4$.

The Fe^{3+} ground term in the O_h crystal field is $^6A_1$ with the five $3d$ electrons in a high-spin configuration $t_{2g}^3 e_g^2$ ($S=5/2$). Whereas this ground state $^6A_1$ in the free ion has a spherical spin distribution, in a crystal structure it is deformed by the effect of the ligand atoms. Since the main deformation will be due to the presence of a water molecule in one of the vertices of the ligand octahedron instead of a halogen atom, a C_4 point symmetry, higher than the actual C_2 symmetry, was assumed for the iron atom, with the symmetry axis collinear with the Fe-O bond. The multipole expansion of the iron spin distribution up to order 4 and which preserves the C_4 point symmetry contains four multipole coefficients. For the ligand atoms, monopolar contributions were assumed. The hydrogen and alkali spin populations in initial fits were below the experimental accuracy and were not included in the final models.

The ζ parameters of the radial part of the atomic multipole expansions are twice the Slater exponents from Refs. 51 and 52. The initial ζ parameters and the n exponents are reported in Table VII. In the fit the ζ parameters of the iron and the

TABLE VIII. Main results of the multipolar expansion spin-density refinement for $K_2FeCl_5 \cdot H_2O$ and $Rb_2FeBr_5 \cdot H_2O$ and the comparison with DFT Mulliken spin populations using the DMOL3 package.

	$K_2FeCl_5 \cdot H_2O$		$Rb_2FeBr_5 \cdot H_2O$	
	Spin-density populations (μ_B)			
	Expt.	DFT	Expt.	DFT
Fe	4.155(2)	4.015	3.973(2)	3.888
*X*1	0.158(3)	0.199	0.227(3)	0.229
*X*2	0.150(1)	0.193	0.176(4)	0.220
*X*3	0.141(3)	0.170	0.167(4)	0.194
*X*4	0.162(3)	0.171	0.195(3)	0.196
O	0.072(3)	0.065	0.064(3)	0.051
H		0.006		0.006
A		0.002		0.007
ζ_{Fe}	7.481(02)		7.909(04)	
ζ_X	4.440(10)		4.433(13)	
n_v	12		12	
χ^2	3.05		3.54	

halogen atoms were allowed to vary and the ζ parameter of the oxygen atom was kept fixed.

Only the magnetic structure factors satisfying the condition that $F_M > 3\sigma$, where σ is the standard deviation, were considered in the refinements of the spin-density distributions, resulting in 200 and 172 magnetic structure factors for the chloride and the bromide compounds respectively. The program used is a modification of MOLLY program.[53]

The main results of the multipolar expansion spin-density refinement for both compounds are listed in Table VIII: the spin-density population normalized to $5\mu_B$ per octahedron, the ζ parameters, the number of parameters of the model represented by n_v, and the agreement factor χ^2 of the fit. Projections of the spin-density reconstruction in the planes containing the Fe−O−H···*X*−Fe pathways are represented in Fig. 3.

The modeling of the spin-density distribution by the multipole expansion approach allowed us to resolve the spin density of the bromine atoms from the spin density of the iron atom, which was not possible in the maximum-entropy method. The spin delocalization from the iron atom is around 17% for $K_2FeCl_5 \cdot H_2O$ and around 21% for $Rb_2FeBr_5 \cdot H_2O$. These values are relatively large in comparison with other spin delocalizations from 3*d* metal ions toward their ligand atoms also studied by PND.[29–37] There are several reasons which can explain this high delocalization. First, both e_g orbitals of the Fe^{3+} ion are semioccupied, allowing the spin transfer through the σ bonding with p_σ orbitals of the ligand atoms, which is more covalent than the π bonding between t_{2g} metal orbitals and p_π ligand orbitals. In addition, trivalent ions are more electronegative than divalent ions, which favors the covalency.

As expected, the spin delocalization toward the bromine atoms is higher than toward the chlorine atoms, which explains why the bromide compounds exhibit higher transition

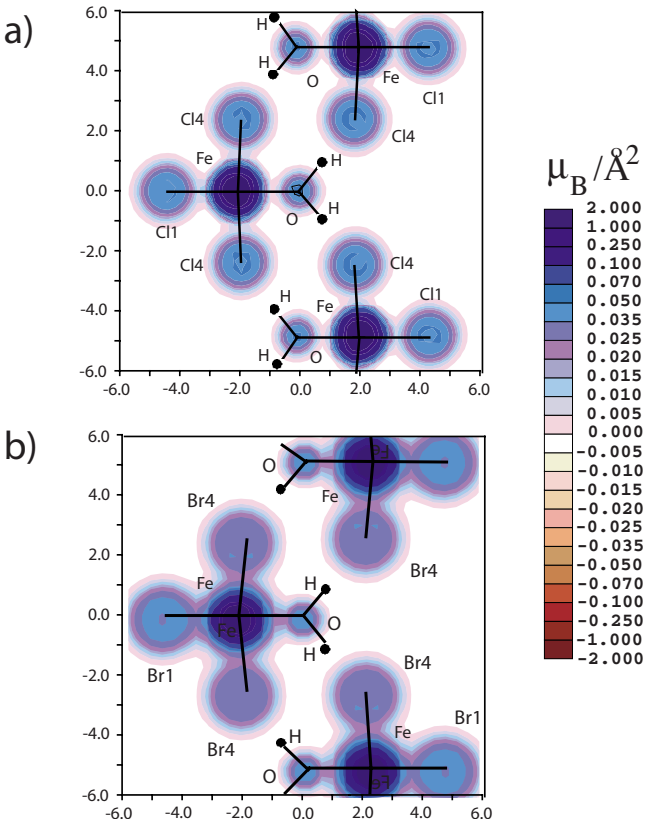

FIG. 3. (Color online) Projection of the spin-density fit in the plane containing the Fe−O−H···*X*−Fe (*X*=Cl, Br) pathway from the multipole expansion approach. (a) $K_2FeCl_5 \cdot H_2O$. (b) $Rb_2FeBr_5 \cdot H_2O$.

temperatures than those of their chloride analogs. On the other hand, the spin population of the oxygen atom is confirmed to be lower than the halogen spin populations, contrary to the hypothesis in the previous analysis of the relative strength of the superexchange pathways.[2] In the previous studies, it was not considered that the oxygen atom is not an O^{2-} ion but an oxygen atom in a water molecule. The latter reduces the covalency between the iron and the oxygen atoms.

A striking result is the value of the spin population of the halogen atom out of the mirror plane. The spin densities of all the halogen atoms are inversely proportional to their bond length to the iron atom except for this atom, whose spin population is higher than that which corresponds to its bond length to the iron atom. An open question is whether this spin-density increase is real, maybe due to the hydrogen bond in which this halogen atom participates, or it is only a spurious effect of the data treatment, maybe due to the different symmetry of this halogen atom.

III. SPIN POPULATIONS DETERMINED BY DFT

It is always interesting to compare the experimental determination of the spin populations from polarized-neutron-diffraction experiments against *ab initio* spin population calculations. In our case this can also help to understand the

experimental results, in particular the role played by the hydrogen atom and the high experimental spin population of the halogen atom which forms a hydrogen bond.

The DMOL3 package[54] was used to perform DFT calculations on the periodic system with the geometries obtained from the nonpolarized-neutron-diffraction experiments. The calculations were performed using both the Perdew-Wang91 exchange-correlation functional[55] and an atom-centered double numeric polarized basis set (DNP). In this basis set, which is the most complete one available in the DMOL3 package, each valence orbital is parameterized by two numerical wave functions and polarization wave functions are also included. These all electron calculations were carried out with the "fine" numerical integration grid of the DMOL3 program and with a multipolar expansion of the charge density for all the atoms up to the octupolar order. The self-consistent energy difference threshold was set up to 10^{-8} a.u. The Mulliken spin populations obtained are listed in Table VIII.

The DFT Mulliken spin populations are in good agreement with the experimental results, being only slightly higher than the latter. The spin populations for the halogen atoms are inversely proportional to the Fe-*X* bond length, even for the halogen atom out of the mirror plane. As for the hydrogen atom, its spin population is very weak. Therefore, DFT calculations do not clarify the nature of the relatively high-spin population of the halogen atoms out of the mirror plane observed in the multipole expansion approach, which maybe should be ascribed to a spurious effect of the fit due to the different point symmetry of these halogen atoms.

IV. CONCLUSIONS

A study of the spin-density distribution in the series $A_2FeX_5 \cdot H_2O$ (A=alkali, NH_4; X=Cl, Br) has been performed on a bromide and a chloride derivative in order to clarify the reasons for the relatively high transition temperatures of the members of this series. The spin-density distribution has been obtained for $K_2FeCl_5 \cdot H_2O$ and $Rb_2FeBr_5 \cdot H_2O$ by polarized neutron diffraction and *ab initio* calculations. The polarized-neutron-diffraction data have been analyzed both by the maximum-entropy method and by a fit to a multipolar expansion of the spin-density distribution. In these compounds there is an important spin-density delocalization from the iron atom toward the ligand atoms. This spin delocalization reflects the fact that the magnetic molecular orbitals are spread over the ligand atoms, thus enhancing the magnetic interactions through a superexchange magnetic interaction mechanism. This enhancement of the magnetic interactions is the cause of the surprisingly high transition temperatures in this series of compounds. The spin delocalization is higher on the bromine atoms than on the chlorine atoms, which explains why the transition temperatures of the bromide compounds are higher than the transition temperatures of their chloride analogs. On the other hand, the existence of a superexchange magnetic interaction mechanism due to a spin delocalization from the iron ion to the ligand atoms also explains the dependency of the ordering temperatures on the radius of the alkali atoms: The bigger the alkali size is, the larger are the distances between the ligand atoms in the superexchange pathways and, therefore, the lower is the ordering temperature.

ACKNOWLEDGMENTS

The work in Zaragoza was supported by Research Grants No. MAT2006-13765-C02-02, No. MAT2007-61621, and No. CSD2007-00010 from the Ministry of Science and Innovation. The Institut Laue-Langevin and the Centre d'Etudes Nucléaires de Grenoble are acknowledged for the allocations of neutron beam time on instruments D9, D10, and D23. We are especially grateful to Eric Ressouche (CENG) for advice on multipole refinements and to John Archer (ILL), Philippe Decarpentrie (ILL), and Pascal Fouilloux (CENG) for technical assistance.

*Present address: Laboratory of Molecular Magnetism, Via della Lastruccia 3, Sesto Fiorentino (FI) 50019, Italy.
†Corresponding author; jcampo@unizar.es

[1] R. L. Carlin and F. Palacio, Coord. Chem. Rev. **65**, 141 (1985).
[2] J. A. Puertolas, R. Navarro, F. Palacio, J. Bartolome, D. Gonzalez, and R. L. Carlin, Phys. Rev. B **31**, 516 (1985).
[3] J. A. Puertolas, R. Navarro, F. Palacio, J. Bartolome, D. Gonzalez, and R. L. Carlin, Phys. Rev. B **26**, 395 (1982).
[4] A. Paduan-Filho, F. Palacio, and R. L. Carlin, J. Phys. (Paris), Lett. **39**, L279 (1978).
[5] F. Palacio, A. Paduan-Filho, and R. L. Carlin, Phys. Rev. B **21**, 296 (1980).
[6] S. Fishman and A. Aharony, J. Phys. C **12**, L729 (1979).
[7] J. Campo, F. Palacio, M. C. Morón, C. Becerra, and A. Paduan-Filho, J. Phys.: Condens. Matter **11**, 4409 (1999).
[8] J. Campo, F. Palacio, A. Paduan-Filho, C. Becerra, M. Fernandez-Díaz, and J. Rodriguez-Carvajal, Physica B (Amsterdam) **234-236**, 622 (1997).
[9] C. C. Becerra, A. Paduan-Filho, T. Fries, Y. Shapira, M. Gabás, J. Campo, and F. Palacio, J. Magn. Magn. Mater. **140–144**, 1475 (1995).
[10] T. Fries, Y. Shapira, A. Paduan-Filho, C. Becerra, and F. Palacio, J. Phys.: Condens. Matter **5**, L107 (1993).
[11] Z. V. Carvalho, C. C. Becerra, A. Paduan-Filho, and F. Palacio, J. Magn. Magn. Mater. **226-230**, 615 (2001).
[12] F. Palacio, M. Gabás, J. Campo, C. C. Becerra, A. Paduan-Filho, and V. B. Barbeta, Phys. Rev. B **56**, 3196 (1997).
[13] A. Tobo, A. Ito, and K. Motoya, J. Phys. Soc. Jpn. **67**, 1784 (1998).
[14] J. N. McElearney and S. Merchant, Inorg. Chem. **17**, 1207 (1978).
[15] C. J. O'Connor, B. S. Deaver, Jr., and E. Sinn, J. Chem. Phys. **70**, 5161 (1979).
[16] R. L. Carlin and C. J. O'Connor, Chem. Phys. Lett. **78**, 528 (1981).
[17] R. L. Carlin, S. N. Bhatia, and C. J. O'Connor, J. Am. Chem.

Soc. **99**, 7728 (1977).
[18] R. L. Carlin and R. Burriel, Phys. Rev. B **27**, 3012 (1983).
[19] T. Smith and S. A. Friedberg, Phys. Rev. **177**, 1012 (1969).
[20] R. L. Carlin, R. Burriel, J. A. Rojo, and F. Palacio, Inorg. Chem. **23**, 2213 (1984).
[21] U. Kambli and H. Güdel, Inorg. Chem. **21**, 1270 (1982).
[22] T. Hamasaki, H. Kubo, A. Millan, and F. Palacio, J. Magn. Magn. Mater. **1**, 1 (2006).
[23] A. Zheludev, V. Barone, M. Bonnet, B. Delley, A. Grand, E. Ressouche, P. Rey, R. Subra, and J. Schweizer, J. Am. Chem. Soc. **116**, 2019 (1994).
[24] J. M. Rawson and F. Palacio, Struct. Bonding (Berlin) **100**, 94 (2001).
[25] J. Campo, J. Luzon, F. Palacio, and J. M. Rawson, in *Carbon-Based Magnetism*, edited by T. Makarova and F. Palacio (Elsevier, New York, 2006), pp. 159–188.
[26] M. Gabás, F. Palacio, J. Rodríguez-Carvajal, and D. Visser, J. Phys.: Condens. Matter **7**, 4725 (1995).
[27] J. Campo, J. Luzon, F. Palacio, G. J. McIntyre, and A. Millan, the following paper, Phys. Rev. B **78**, 054415 (2008).
[28] J. B. Forsyth, in *Electron and Magnetization Densities in Molecules and Crystals*, edited by P. Becker (Plenum, New York, 1980), pp. 791–819.
[29] B. E. F. Fender, B. N. Figgis, J. B. Forsyth, P. A. Reynolds, and E. Stevens, Proc. R. Soc. London, Ser. A **404**, 127 (1986).
[30] B. E. F. Fender, B. N. Figgis, and J. B. Forsyth, Proc. R. Soc. London, Ser. A **404**, 139 (1986).
[31] R. J. Deeth, B. N. Figgis, J. B. Forsyth, E. S. Kucharski, and P. A. Reynolds, Proc. R. Soc. London, Ser. A **421**, 153 (1989).
[32] B. N. Figgis, J. B. Forsyth, E. S. Kucharski, P. A. Reynolds, and F. Tasset, Proc. R. Soc. London, Ser. A **428**, 113 (1990).
[33] R. J. Deeth, B. N. Figgis, J. B. Forsyth, E. S. Kucharski, and P. A. Reynolds, Proc. R. Soc. London, Ser. A **436**, 417 (1992).
[34] B. N. Figgis and P. A. Reynolds, Mol. Phys. **80**, 1377 (1993).
[35] G. S. Chandler, B. N. Figgis, R. A. Phillips, P. A. Reynolds, R. Mason, and G. A. Willians, Proc. R. Soc. London, Ser. A **384**, 31 (1982).
[36] B. N. Figgis, P. A. Reynolds, and R. Mason, Proc. R. Soc. London, Ser. A **384**, 49 (1982).
[37] F. A. Wedgwood, Proc. R. Soc. London, Ser. A **349**, 447 (1976).
[38] P. J. Brown, B. N. Figgis, and P. A. Reynolds, J. Phys.: Condens. Matter **2**, 5297 (1990).
[39] B. N. Figgis, P. A. Reynolds, and R. Mason, Inorg. Chem. **23**, 1149 (1984).
[40] R. Papoular and B. Gillon, Europhys. Lett. **13**, 429 (1990).
[41] P. J. Brown, A. Capiomont, B. Gillon, and J. Schweizer, J. Magn. Magn. Mater. **14**, 289 (1979).
[42] A. Bellanca, Period. Mineral. **18**, 59 (1948).
[43] A. Schultz and R. L. Carlin, Acta Crystallogr., Sect. B: Struct. Sci. **B51**, 43 (1995).
[44] J. C. Matthewman, P. Thompson, and P. J. Brown, J. Appl. Crystallogr. **15**, 167 (1982).
[45] M. P. Gupta, S. M. Prasad, and B. Yadav, Cryst. Struct. Commun. **1**, 211 (1972).
[46] P. Becker and P. Coppens, Acta Crystallogr., Sect. A: Cryst. Phys., Diffr., Theor. Gen. Crystallogr. **A30**, 129 (1974).
[47] $R=\Sigma(|F_0|-|F_c|)/\Sigma|F_0|$; $R_w=[\Sigma w(|F_0|-|F_c|)^2/\Sigma w|F_0|^2]^{1/2}$; $\chi^2=\Sigma(|F_0|-|F_c|)^2/\sigma^2$.
[48] $\exp[-\frac{1}{4}(\beta_{11}h^2a^{*2}+\beta_{22}k^2b^{*2}+\beta_{33}l^2c^{*2}+2\beta_{12}ha^*kb^*+2\beta_{13}ha^*lc^*+2\beta_{23}kb^*lc^*)]$, where h, k, and l are the reflection indices and a^*, b^*, and c^* are the reciprocal cell parameters.
[49] S. F. Gull and J. Skilling, *MemSys3 (Quantified Maximum Entropy Subroutine Library)* (Maximum Entropy Data Consultants, Meldreth, UK, 1989).
[50] E. Ressouche, J. X. Boucherle, B. Gillon, P. Rey, and J. Schweizer, J. Am. Chem. Soc. **115**, 3610 (1993).
[51] W. J. Hehre, R. F. Stewart, and J. A. Pople, J. Chem. Phys. **51**, 2657 (1969).
[52] W. J. Hehre, R. Ditchfield, R. F. Stewart, and J. A. Pople, J. Chem. Phys. **52**, 2769 (1970).
[53] N. K. Hansen and P. Coppens, Acta Crystallogr., Sect. A: Cryst. Phys., Diffr., Theor. Gen. Crystallogr. **A34**, 909 (1978).
[54] B. Delley, J. Chem. Phys. **92**, 508 (1990).
[55] J. P. Perdew, J. A. Chevary, S. H. Vosko, K. A. Jackson, M. R. Pederson, D. J. Singh, and C. Fiolhais, Phys. Rev. B **46**, 6671 (1992).